Soft Matter

Cite this: *Soft Matter*, 2011, **7**, 5423

www.rsc.org/softmatter

PAPER

Arrest of morphological transformation during evaporation-induced self-assembly of mixed colloids in micrometric droplets by charge tuning

Debasis Sen,*[a] Jose Savio Melo,[b] Jitendra Bahadur,[a] Subhasish Mazumder,[a] Shovit Bhattacharya,[c] Stanislaus Francis D'Souza,[b] Henrich Frielinghaus,[d] Günter Goerigk[d] and Rudolf Loidl[e]

Received 19th January 2011, Accepted 6th April 2011
DOI: 10.1039/c1sm05100h

Self-assembled grains of mixed colloids have been synthesized using evaporation induced self-assembly (EISA) by spray drying. We demonstrate using electron microscopy and small-angle neutron scattering experiments that buckling driven sphere to deformed-doughnut like morphological transformation in such a process can be arrested by proper tuning of the surface charge on the colloidal components. The buckling amplitude diminishes with a reduction in stabilization force between the colloidal particles. It is established that such arrest of morphological transformation is related to an effective exposure of the surface of softer component at gas–liquid interface. Scattering experiments confirm relatively more compact structure of the non-buckled grains compared to that of the buckled grains. A plausible mechanism regarding the arrest of morphological transformation by surface charge tuning is illustrated.

Introduction

During the last few years, evaporation-induced self-assembly (EISA) of nanoparticles has attracted a great deal[1–14] of attention. This is because of the fact that EISA provides a fast as well as an effective way to synthesize important functional materials such as colloidal-crystals, tunable porous grains, nano-composite microcapsules, *etc.* that have potential applications in pharmaceutical, chemical and in other industries. In practice, this is realized by a popular technique, known as spray drying, where micrometric colloidal droplets get transformed into solid powder grains with assembled hierarchical structures in a short duration of time. Due to blended co-existence of both fluidic and elastic behaviors of droplets in course of drying, droplets often undergo striking morphological transition due to mechanical instabilities, such as buckling, fracture, *etc.* Such instabilities are primarily governed by various physico-chemical environments during the drying process. Depending on the time-scale of drying, a colloidal droplet becomes viscoelastic and may either store energy in elastic deformation or may relieve stress through viscous flow while the solvent evaporates. Because of such instabilities, an initial spherical liquid droplet gets transformed into a buckled doughnut or mushroom like powder grain during assembly. Several physicochemical factors, such as, the rate of drying, the size of colloidal particles and interactions between them, the nature of solvent, *etc.*, play a role in effecting such instabilities. In recent past, the physical origin of such buckling instabilities has been dealt with[1–3] for a suspension of single type of colloidal particles only. However, such instability for a multi-component system has not been addressed so far to the best of our knowledge. Further, a method to arrest such morphological transformation is yet to be proposed.

In this paper, we demonstrate that the buckling instabilities during drying of droplets of the mixed colloidal suspension can be arrested by tuning the surface charge on the colloidal components. Further, interestingly, the buckling gets diminished as the effective repulsive stabilizing force between the colloidal particles is reduced and the buckling gets fully arrested when the polarity of the surface charge of two components becomes opposite in nature. This observation is in contrast to that which has been observed[1] in the case of drying of sessile droplets consisting of single type of colloidal particles only. Present investigation also indicates that the effective elastic modulus of the particles exposed at the air–water interface plays an important role in controlling the buckling deformation.

In recent past, in a pioneering work[1] by Tsapis *et al.*, the following has been conjectured[1] in relation to the buckling of drying droplet that contains colloidal particles of single type. After an initial period of isotropic shrinkage, a shell of jammed colloidal particles is formed at the air–water interface. The inner core of the droplet remains at nearly its initial volume fraction, ϕ_i, while a shell with volume fraction ϕ_c (where $\phi_c \gg \phi_i$) forms. If the effective repulsive potential between the colloidal particles is significant enough, the constituent particles can roll and

[a]*Solid State Physics Division, Bhabha Atomic Research Centre, Mumbai, 400085, India. E-mail: debasis@barc.gov.in*
[b]*Nuclear Agriculture and Biotechnology Division, Bhabha Atomic Research Centre, Mumbai, 400085, India*
[c]*Technical Physics and Prototype Engineering Division, Bhabha Atomic Research Centre, Mumbai, 400085, India*
[d]*Julich Centre for Neutron Science, FRM-II, Garching, Germany*
[e]*Atominstitut der Osterreichischen Universitaten, A-1020 Wien, Austria*

rearrange themselves in such a manner that leads to droplet shrinkage in an isotropic fashion[14] during drying. However, if the stabilizing electrostatic repulsive forces between the particles are not strong enough, at some particular instant of time, the rearrangement of the particles stops and the droplet does not shrink further although the evaporation of the liquid continues through the porous shell. In such a situation, at some instance, the capillary forces overcome the stabilizing electrostatic forces between the particles and buckling occurs[1] at a critical thickness of the shell.

Further, in the present case, we demonstrate that the buckling criteria for drying droplets of mixed colloidal particles remain beyond the existing buckling hypothesis as mentioned above.

Experimental section

We performed EISA of mixed colloidal droplets that consist of colloidal silica (~15 nm, VISA Chemicals, Mumbai, India) and *Escherichia coli* (*E. coli*, grown in Luria Bertani broth at 37 °C overnight under shaking) suspension using spray drying (LU 222, LABULTIMA). The mass fraction of silica and wet *E. coli* in the initial suspension (*i.e.*, before drying) was 2 wt% and 6 wt %, respectively. All the spray dried samples were calcined at 300 °C for 10 h to remove the organic moieties. The ζ-potential (Malvern Zetasizer 3000) for individual silica and virgin *E. coli* suspensions was found to be −43.2 mV and −30.0 mV, respectively. The same for the mixed suspension of silica and *E. coli* was −58.6 mV. A typical morphology of the spray dried grains for this case is shown in Fig. 1a. It is evident that the grains are fully buckled (Case-I) and look like deformed doughnuts with multi-invagination zones.

In order to tune the repulsive force between the colloidal particles, *E. coli* cells were treated to impart a polycationic charge on the cell surface[15] using polyethylenimine (PEI) (Sigma Chemical Co., MO, USA, average $M_w \approx 7.5 \times 10^5$). In fact, *E. coli* cells were treated with PEI 0.2, 1 and 2%, respectively by stirring the suspension for 30 minutes following which the cells were harvested by centrifugation and washed in order to remove the unbound and free PEI. It has been verified by the Ostwald method that the specific viscosity of 2% PEI solution with respect to pure water is 1.5 only. It is needless to say that the effective viscosity will be even smaller after removal of excess PEI. ζ-Potentials (Malvern Zetasizer 3000) for *E. coli* suspensions with varying PEI coating (0.2, 1.0, 2.0%) at the surface of *E. coli* were found to be −8.4 mV (Case-II), +14.6 mV (Case-III) and +19.6 mV (Case-IV), respectively. This confirms that the adsorbed layer of PEI on *E. coli* surface decreases the negative charge and eventually reverses the polarity of surface charge on *E. coli*, depending on the amount of polymer coated. Spray drying experiments (with identical experimental conditions as those for the previous experiment) were performed with silica and PEI coated *E. coli* mixed colloidal suspension. The micrographs of the obtained spray dried grains (after calcinations at 300 °C for 10 h) are depicted in Fig. 1b–d, respectively. Reproducibility of the observations was verified.

To obtain small-angle neutron scattering (SANS) data over a wide scattering-vector (q) range, an essential requirement to probe such hierarchically structured grains, scattering experiments have been performed at three different instruments

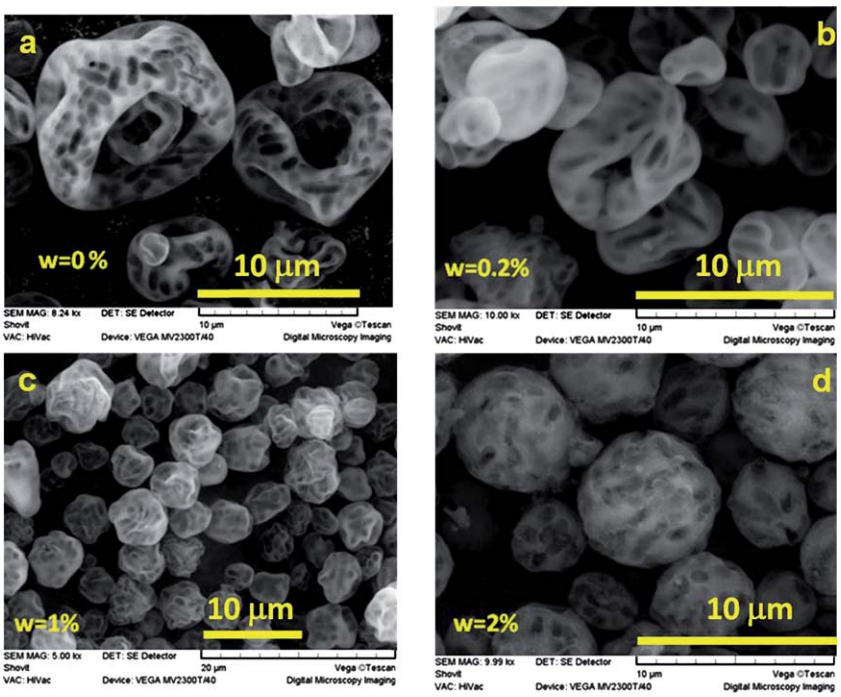

Fig. 1 Scanning electron micrographs of self-assembled grains synthesized with silica colloids and *E. coli* suspension. (a) Buckling of the drying droplets is maximum when *E. coli* is not covered with poly-cationic PEI. It is clearly observed that buckling reduces with increase in the amount of coated PEI, *i.e.*, by reducing the repulsive forces between the colloidal particles. (b) *E. coli* coated with 0.2% PEI, (c) *E. coli* coated with 1.0% PEI and (d) *E. coli* coated with 2.0% PEI.

namely, KWS-1[25] and KWS-3[26] (at JCNS, FRM-II, Garching, Germany) and S18[27] (at ILL, Grenoble, France). Scattering data over a wide range of wave vector transfer (0.00002–0.2 $Å^{-1}$) were obtained using the above facilities after performing some preliminary experiments using SANS instruments[28,29] at DHRUVA, Trombay, India. SEM micrographs were obtained using a VEGA, TeScan instrument.

Results and discussion

It is worth mentioning that the quantitative measure of the strength of drying is expressed by the Peclet number (P_e), which is defined as the ratio of R^2 and $D\tau_{dry}$, where R is the radius of the droplets, D is the diffusion coefficient of the colloidal particles in the droplet and τ_{dry} is the drying time. If $P_e \ll 1$, the drying process is regarded[14] as slow and the droplets shrink isotropically[14] throughout the drying process leading to a completely jammed spherical grain of nanoparticles. However, for $P_e \gg 1$, the drying is fast enough and that often leads to formation of hollow and buckled grains. Diffusion coefficient (D) may be calculated from the Einstein–Stokes relation, $D = K_BT/6\pi\eta r$, where K_B is Boltzmann constant, η is the viscosity and 'r' represents the radius of the colloids. For $T = 40\ ^\circ C$, $r = 7$ nm for the silica colloids (as observed from scattering techniques) and $\eta = 6.53 \times 10^{-4}$ Pa s (the viscosity of pure water at 313 K) D works out to be $5.849 \times 10^{-11}\ m^2\ s^{-1}$. The value of the same for *E. coli* turns out to be $5.570 \times 10^{-13}\ m^2\ s^{-1}$. The drying time ($\tau$) can be calculated using the geometry of drying chamber and gas flow rate and the same was found to be 0.36 s. Thus, the Peclet number becomes 1.2 for a droplet containing only silica colloid. The same turns out to be 125 for droplet containing only *E. coli*. Thus, the addition of *E. coli* in silica suspension effectively increases the Peclet number *vis-a-vis* the instability of the droplet.

It is interesting to note from the ζ-potential measurements that both silica and virgin *E. coli* possess charge of similar polarity (−ve) and thus form a repulsive system. It is clearly evident from the SEM micrographs that the amplitude of buckling has been maximum in Case-I, *i.e.*, when the repulsive force between the colloids has been maximum (both silica and *E. coli* possess negative polarities of −43.2 mV and −30.0 mV, respectively). However, the buckling amplitude reduces with decrease in the repulsive stabilization force (by coating poly-cationic PEI on *E. coli*). Gradually, the buckling becomes insignificant and eventually vanishes when the system becomes somewhat attractive (the ζ-potential for silica is −43.2 mV and 2% PEI coated *E. coli* is +19.6 mV) by reversing the polarity of the surface charge of *E. coli*. According to the existing hypothesis,[1,2] the evolution should have been in the other way, *i.e.*, the grains should have been more hollow and deformed when the stabilization force is reduced by making the system slightly attractive. This observation motivated us to search for the mechanism of buckling and its arrest in the case of EISA of mixed colloids. At this juncture, it is worth mentioning that the duration of each spray drying experiment has been nearly half an hour and there has been no visible flocculation or phase separation of the colloids within this time interval even for the maximum attractive system (2% PEI coated *E. coli*). It is also important to mention that such unusual colloidal stability[16] that is beyond the explanation by normal DLVO formalisms[17,18] is well known in the literature[16] in several cases.

One interesting point to note at this juncture is that *E. coli* is softer (longitudinal Young's modulus ≈ 25 MPa and circumferential Young's modulus ≈ 75 MPa, density ≈ 1.1 gm cm^{-3})[19] than silica (∼75 000 MPa, density ≈ 2.0 gm cm^{-3} for colloidal silica and ∼2.5 gm cm^{-3} for bulk silica). In fact, the present investigation was also motivated by the query whether the buckling could be arrested by modifying the effective elastic strength of the shell at the air–water interface for a mixed colloidal system. In addition, one can perceive from everyday experience that a soft stem can be bent with ease but it is not easy to do so when the stem is inserted in a hard and hollow rod. When *E. coli* is not coated with PEI, *i.e.*, in Case-I, the repulsive stabilization force is maximum between silica and *E. coli*. Thus, the air–water interface of the droplets is equally exposed to silica and *E. coli*. As the elastic constant of *E. coli* is significantly small compared to that of silica, the suspension droplet of *E. coli* and silica is more prone to buckling in this case than where the air–water interface is exposed only to silica. Here, it is worth mentioning that the spray dried grains (Fig. 2) synthesized from silica colloids (2 wt%) alone are either smooth doughnuts with two small dimples or almost spherical but are not deformed as in Case-I. When PEI is coated on *E. coli*, the negative charge of virgin *E. coli* gets reduced and gradually attains positive polarity at higher PEI concentration. In such an environment, the silica particles, which are much smaller than *E. coli*, form a particle-cloud around *E. coli*. Thus, during drying, the air–water interface is mostly exposed to silica and hence the amplitude of buckling gets diminished. It is also supported by the micrograph (Fig. 1d) that the cylindrical pores in the grains, as templated by *E. coli*,

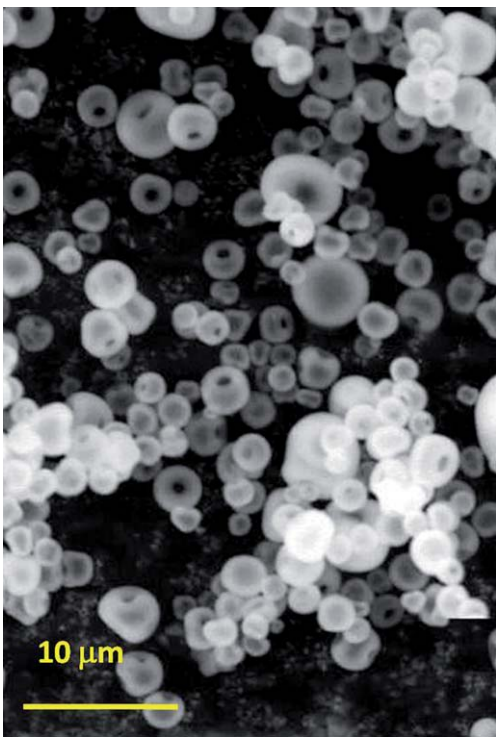

Fig. 2 Scanning electron micrographs of self-assembled grains of only silica colloid. It is evident that the grains are either just about to be smooth doughnuts or nearly spherical but no deformed doughnut is observed as is observed for the silica–*E. coli* system.

look somewhat blurred in this case because of the fact that *E. coli* gets mostly covered with silica nanoparticles. Thus, in this case, the buckling could be stopped by not exposing *E. coli*, the softer component, directly to the air–water interface. The situation is represented schematically in Fig. 3.

As the arrest of buckling is strongly associated with the modification of the hierarchical structure of the assembled grains, the same has also been verified by use of scattering measurements which gives statistically averaged information from bulk. In our work, we have employed small-angle neutron scattering (SANS) measurements to unravel this enigma. It is understandable that the assembled grains possess structure in three different length scales due to the presence of (i) silica particles, (ii) pores as templated by *E. coli* and (iii) overall assembled grains. Here comes the importance of SANS. Small-angle scattering[20–24] is a unique technique to measure the internal structure of such assembled grains in a true statistical sense unlike the microscopy techniques. Variation of scattering intensity with wave-vector transfer (q) for the spray dried samples is plotted in Fig. 4. The scattering intensities were put in absolute scale by measuring the effective solid thickness[30] from the transmission measurements. Three distinct zones in scattering profiles, zone-III, zone-II and zone-I, respectively bear the signatures of the above mentioned length scales in the grain, respectively. This is because of the fact that the information about the bigger structure manifests at the smaller wave vector transfer region in a scattering measurement. It is to be noted here that three different SANS facilities were used to cover a wide q range as needed for such spray dried grains. The scattering data for zones-II and III were obtained using SANS facilities (KWS-1 and KWS-3) that are equipped with position sensitive detectors (PSD). It is needless to say that the use of PSD allows good

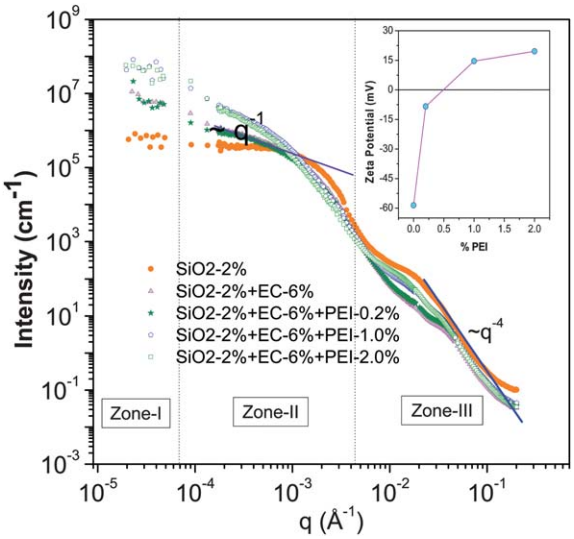

Fig. 4 SANS data from the hierarchically structured assembled grains. Three different length scales in the assembled grains are obvious from the scattering data. It is observed from the data that the correlation of the particles inside the grains gets modified with change in the surface charge of *E. coli*.

statistics of data. However, such instruments cannot access very low q region because of the finite size and the divergence of direct beam. Hence, the double crystal based ultra small-angle neutron scattering (USANS) instrument (S18) was used to access the data at very low q region (zone-I). In general, a double crystal based instrument,[27] unlike PSD based instrument, uses step by step rotation of the analyser crystal for collection of data at low q value. Further, the flux at sample position for such instrument is

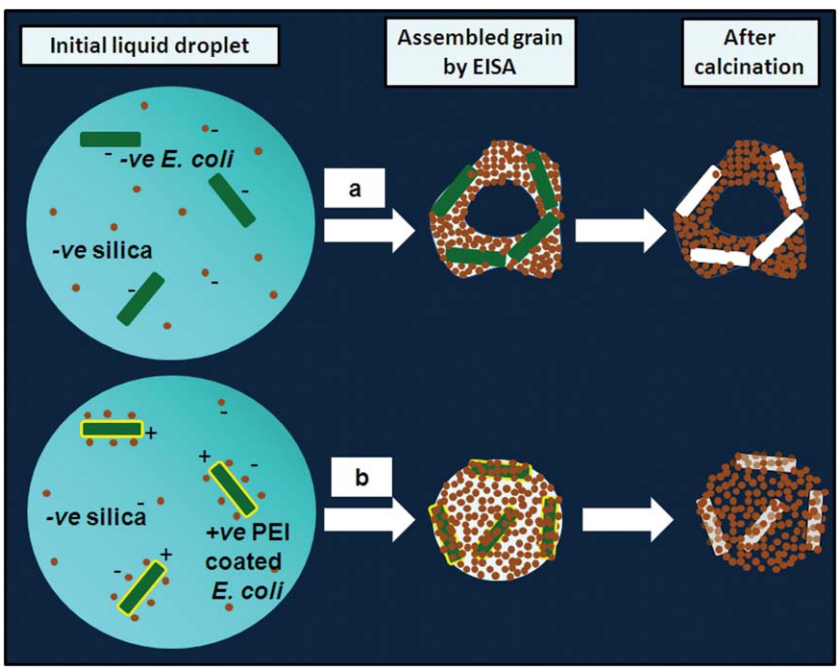

Fig. 3 Schematic representation of the assembly process of silica and *E. coli*. (a) Both silica and *E. coli* have negative surface charges and the system is repulsive. The assembled grains are deformed. (b) Silica is negative as in earlier case but the *E. coli* surface is coated with PEI to impart positive charge on the *E. coli* surface. The assembled grains are spherical in this case and no buckling has occurred. This is in contrast to the existing hypothesis of buckling.

limited[27] because of the requirement of usage of nearly perfect monochromator crystal. Thus the statistics of data is not as good as that is obtained with PSD based instrument for zones-II and III. However, the trend of USANS profile matches in a reasonable fashion to the data in the next zone.

It is obvious from Fig. 4 that the functionality of scattering profiles gets modified with the addition of *E. coli* and also by further charge modification. SEM could not resolve individual silica particles due to resolution constraint but zone-III of the SANS profiles indeed shows their existence. The q^{-1} behaviour of the scattering profile in zone-II (in the q range of 10^{-4} to 10^{-3} Å^{-1}) indicates the presence of cylindrical macropores templated by *E. coli*. It is to be noted that such region with q^{-1} dependence of scattering data was totally absent for sample with only silica without *E. coli*. It is interesting to observe from the scattering profiles that the intensity in zone-III (*i.e.*, the scattering contribution from silica nanoparticles) gets reduced significantly when unmodified virgin *E. coli* is added to silica suspension. With increase in the amount of added PEI, the intensity in zone-III starts increasing again. This signifies the appearance of relatively more compact grains in Cases-II, III and IV than in Case-I.

In a quantitative way, the scattering intensity from such hierarchical grains may be approximated[31–33] by additive contributions of scattering components from three different length scales[31,32] and can be represented as:

$$I(q) = C_S\Delta\rho_S^2 I_S(q) + C_p\Delta\rho_{pore}^2 I_{pore}(q) + C_g\Delta\rho_g^2 I_g(q) + B \quad (1)$$

If ρ_S is the scattering length density of silica then $\Delta\rho_S = \rho_S - \rho_{int}$ (ρ_{int} being the scattering length density of interstices between silica colloids). As interstice between silica colloids is air, $\rho_{int} = 0$ and hence $\Delta\rho_S$ can be taken equal to ρ_S. Here, $\Delta\rho_g$ represents the average scattering contrast of the grains hence $\Delta\rho_g = \phi_S\Delta\rho_S + \Delta\rho_{int}$. As the medium in which the grains are embedded and the medium of the interstices are both air in this case, $\Delta\rho_{int} = 0$ and thus $\Delta\rho_g = \phi_S\Delta\rho_S$. B represents background. After calcination of the grains, at 300 °C for 10 h, most of the organic moieties escape from the grains (as verified from weight measurements before and after calcination) and hence, in the present case, $\Delta\rho_{pore}$ has been taken as $\Delta\rho_S$ itself. C_s, C_p and C_g are scale factors scattering contribution from silica, pore and grain, respectively. For totally compact arrangement of the particles in a grain, which happens only in the case of isotropic shrinkage under slow drying,[14] these constants are nothing but the global volume fraction of the individual components in a grain. $I_s(q)$ is the scattering contribution from the silica particles. Assuming an interacting polydisperse spherical particle model $I_s(q)$ in eqn (1), under local monodisperse approximation,[34] may be expressed as:

$$I_s(q) = \frac{\int_0^\infty P_S(q,r)D(r)v^2(r)S(q,r)\mathrm{d}r}{\int_0^\infty v(r)D(r)\mathrm{d}r} \quad (2)$$

In eqn (2) $P_s(q, r)$ represents the form factor of the silica particles of radius 'r', $D(r)$ represents the size distribution of these particles with radius 'r' and volume $v(r)$. $S(q, r)$ represents the structure factor due to the interparticle arrangement of these particles. It is to be mentioned that $S(q, r)$ corresponding to a sticky hard sphere type potential resulted in a better representation of the experimental data compared to that of only hard sphere potential. At this juncture, it is to be mentioned that the exact nature of the inter-particle arrangement and corresponding $S(q, r)$ for such grains are not clearly understood so far. What has been understood so far is that as the water goes out of the droplet during drying, the colloidal particles come closer because of the attractive capillary forces and finally get jammed. Such attractive nature of capillary force may arrange the particles in such a way (of course not a fractal at the same time) that the interparticle-correlation does not correspond to that of the exact hard sphere repulsive potential. We observed that neither the exact hard sphere repulsive correlation nor the fractal correlation could fit the data well. At the same time a sticky hard sphere model produces a better agreement. Thus, as an approximation, we used a sticky hard sphere model for this case and it worked well. Expression for $I_{pore}(q)$ due to the presence of templated macropores is similar to that of $I_s(q)$ except the fact that a cylindrical form factor for the macropores has been used in this case (to account for q^{-1} behaviour in zone-II, a signature of the presence of cylindrical pores, and further supported by observation of cylindrical macro-pores from SEM micrographs). Scattering contribution, $I_g(q)$, from overall grains, is manifested in zone-I (except that for the sample with only silica *i.e.*, without *E. coli* for which the scattering profile approaches a Guinier region already at zone-II). A polydisperse spherical particle model was assumed for this term. The estimated parameters from the fitting of the model to the scattering profiles are tabulated in Table 1. The fit of the model to the scattering data is shown in Fig. 5. From the nature of eqn (1), it is clearly evident that the analysis of SANS data for such systems is quite complex. However, it is evident that the above mentioned model fits all the scattering profiles reasonably well over the entire accessible q range. It is seen from the table that the mean size of the grains increases significantly in the presence of *E. coli* as they become hollow and buckled. Further, the mean size and the polydispersity get somewhat reduced when the charge on *E. coli* is modified by PEI as the grains become relatively more compact. The increase of the ratio C_S/C_P with *E. coli* surface modification indicates that the grains become relatively more compact with coating of positive PEI. It is also seen that the grain radius decreases slightly with increases in addition of PEI that occurs because of some compaction in the internal structure. It is worth discussing the following points in regard to the SANS data analysis. The grains in the case of 0% PEI, as seen from the SEM micrograph (Fig. 1a), are very irregular. Thus in this case, there exist polydispersity both in shape as well as in size of the grains. This leads to effective larger polydispersity as far as the SANS data are concerned. With increase in coating amount of PEI, at least the shape polydispersity is removed. This results to a slight decrease in the effective polydispersity with increase in PEI amount. Further, although the SEM is a direct method, it gives only local information but SANS probes bulk material and hence gives a statistically averaged information. We would like to mention that the shape of the SANS profile for the sample with only silica (without *E. coli*) is quite different in zone-I and zone-II. It is significantly broader than the other profiles in zones-I and II.

Table 1 Structural parameters obtained from SANS analysis

	Assembled grain size distribution		Templated cylindrical macro-pore			
Sample	Mean radius (R_{grain})/nm	$\Delta R_{grain}/R_{grain}$	Length (L_{pore})/nm	Average radius (R_{pore})/nm	$\Delta R_{pore}/R_{pore}$	C_S/C_P
Only silica	200	0.099	—	—		—
Silica + EC	2394	0.658	2000	102	0.205	1.2
Silica + EC + PEI 0.2	2266	0.533	2050	115	0.209	2.1
Silica + EC + PEI 1.0	2266	0.533	2600	167	0.305	2.4
Silica + EC + PEI 2.0	2159	0.531	2600	167	0.305	2.5

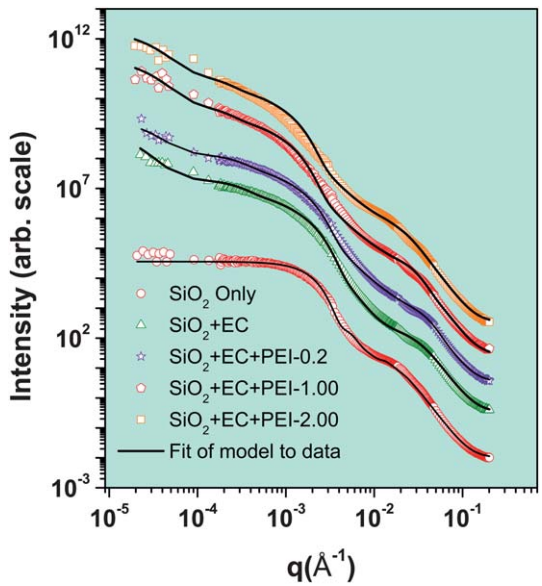

Fig. 5 Fitting of the mesoscopic hierarchical structure model to the SANS data. The profiles are shifted vertically for clarity.

It reached the Guinier region early in zone-II and much before than the other profiles reach. Thus analysis of this profile results in a grain size which is much smaller than that obtained from the other profiles. It is discernible from the SANS data that the zones-I and II get significantly modified when *E. coli* is present (coated or uncoated) in the grains. The q^{-1} dependence of scattering data appears in the profile (in range 10^{-3} to 10^{-4} Å^{-1}), which was not present at all in the case of only silica. The profiles approach towards a Guinier like region in zone-I. Thus the estimated grain sizes in these cases (where *E. coli* template pores have been present) are significantly larger than in the case with only silica.

It may appear at first sight that such arrest of morphological transformation in the present case may be either due to charge effect or due to modification in viscoelastic behavior when PEI is added. However, these two possibilities are differentiated in the following way, in order to reach a plausible conclusion. First of all, it should be noted that the excess or unbound PEI that did not get coated on *E. coli* was removed by washing. As mentioned earlier it was verified that the specific viscosity of 2% PEI solution with respect to pure water is 1.5 only. After removal of excess PEI, it would be even smaller. Thus, there should not be any significant increase in viscosity with PEI coating. Even if it is assumed that the viscosity (η) would increase with coating of PEI, this will certainly lead to a reduction in diffusion coefficient (D) because of the fact that D is inversely related to the viscosity (η). This in turn will increase the value of the Peclet number (P_e) as it is inversely related to D (*i.e.*, $P_e = R^2/D\tau_{dry}$). An increase in P_e value, according to the existing hypothesis, will lead to more hollow and deformed grains. However, our observation in the present case is just the opposite, *i.e.*, the grains become more spherical and more compact with increase in PEI coating. Further, earlier studies[35,36] show that the stability of *E. coli* is not modified by PEI. In addition, it has been found that PEI did not exert any direct bactericidal effect on Gram-negative bacteria when applied alone, even in concentrations far above those required for sensitization. Thus, we believe that such morphological transformation gets arrested through effective coverage of larger and softer colloidal component by smaller and harder component by proper tuning of the surface charge.

Conclusions

In summary, it is revealed that the buckling driven sphere to deformed-doughnut like morphological transformation of mixed colloidal suspension droplets during EISA can be arrested through effective coverage of larger and softer colloidal component by smaller and harder component by proper tuning of the surface charge. Such observations on EISA of mixed colloids are beyond the existing hypothesis of buckling of colloidal suspension droplets that contain only one type of particles. Further, the present work opens up an effective experimental as well as a theoretical route towards the comprehensive understanding of the buckling phenomenon during EISA of mixed colloids.

Acknowledgements

Authors thank Dr S. Ramanathan of MSD, BARC for his kind help in ζ-potential measurements. DS would like to thank Drs Antoine Thill and Olivier Spalla of LIONS, SCM, DRECAM, CEA Saclay, France for many fruitful discussions on spray drying during his visit at CEA Saclay, France. DS and JB thankfully acknowledge financial support (DST(5)/AKR/P087/10-11/673) received from Department of Science and Technology, India through S. N. Bose National Centre for Basic Science, Kolkata, India for neutron scattering work at JCNS, Germany and ILL, France.

References

1 N. Tsapis, E. R. Dufresne, S. S. Sinha, C. S. Riera, J. W. Hutchinson, L. Mahadevan and D. A. Weitz, *Phys. Rev. Lett.*, 2005, **94**, 018302.

2 N. Tsapis, D. Bennett, B. Jackson, D. A. Weitz and D. A. Edwards, *Proc. Natl. Acad. Sci. U. S. A.*, 2002, **99**, 12001.
3 L. Pauchard and Y. Couder, *Europhys. Lett.*, 2004, **66**(5), 667–673.
4 F. Iskandar, Mikrajuddin and K. Okuyama, *Nano Lett.*, 2001, **1**, 231–234.
5 D. Sen, S. Mazumder, J. S. Melo, A. Khan, S. Bhattyacharya and S. F. D'Souza, *Langmuir*, 2009, **25**(12), 6690–6695.
6 C. Boissiere, D. Grosso, A. Chaumonnot, L. Nicole and C. Sanchez, *Adv. Mater.*, 2011, **23**, 599–623.
7 S. Lyonnard, J. R. Bartlett, E. Sizgek, K. S. Finnie, T. Zemb and J. L. Woolfrey, *Langmuir*, 2002, **18**, 10386–10397.
8 D. Sen, O. Spalla, L. Belloni, T. Charpentier and A. Thill, *Langmuir*, 2006, **22**, 3798–3806.
9 Y. Lu, H. Fan, A. Stump, T. L. Ward, T. Rieker and C. J. Brinker, *Nature*, 1999, **398**, 223–226.
10 F. Iskandar, I. W. Lenggoro, B. Xia and K. Okuyama, *J. Nanopart. Res.*, 2001, **3**, 263–270.
11 M. T. Bore, S. B. Rathod, T. L. Ward and A. K. Datye, *Langmuir*, 2003, **19**, 256–264.
12 F. Iskandar, L. Gradon and K. Okuyama, *J. Colloid Interface Sci.*, 2003, **265**, 296–303.
13 O. D. Velev, A. M. Lenhoff and E. W. Kaler, *Science*, 2000, **287**, 2240–2243.
14 D. Sen, O. Spalla, O. Taché, P. Haltebourg and A. Thill, *Langmuir*, 2007, **23**, 4296–4302.
15 J. S. Melo and S. F. D'Souza, *World J. Microbiol. Biotechnol.*, 1999, **15**, 17–21.
16 J. M. Peula, A. Fernández-Barbero, R. Hidalgo-Álvarez and F. J. de las Nieves, *Langmuir*, 1997, **13**, 3938–3943.
17 B. V. Derjaguin and L. D. Landau, *Acta Physicochim. URSS*, 1941, **14**, 633.
18 E. J. W. Verwey and J. T. G. Overbeek, *Theory of Stability of Lyophobic Colloids*, Elsevier, Amsterdam, 1948.
19 G. Lan, C. W. Wolgemuth and S. X. Sun, *Proc. Natl. Acad. Sci. U. S. A.*, 2007, **104**, 16110–16115.
20 O. Glatter and O. Kratky, *Small Angle X-ray Scattering*, Academic Press, London 1982.
21 P. Linder and T. Zemb, *Neutrons, X-Rays and Light: Scattering Methods Applied to Soft Condensed Matter*, Elsevier, Amsterdam, 2002.
22 D. Sen, S. Mazumder and J. Bahadur, *Phys. Rev. B: Condens. Matter Mater. Phys.*, 2009, **79**, 134207.
23 S. Mazumder, D. Sen, A. K. Patra, S. A. Khadilker, R. M. Cursetji, R. Loidl, M. Baron and H. Rauch, *Phys. Rev. Lett.*, 2004, **93**, 255704.
24 S. Mazumder, D. Sen, I. S. Batra, R. Tewari, G. K. Dey, S. Banerjee, A. Sequeira, H. Amentisch and S. Bernstorff, *Phys. Rev. B: Condens. Matter*, 1999, **60**, 822.
25 H. Frielinghaus, *et al.*, *JCNS Experimental Report*, 2007/2008. http://www.jcns.info/src/report/sr2008_KWS1_new_PB3.pdf.
26 G. Goerigk, et al, *JCNS Experimental Report*, 2007/2008, http://www.jcns.info/src/report/sr2008_KWS3tex.pdf; G. Goerigk and Z. Varga, *J. Appl. Crystallogr.*, 2011, **44**, 337–342.
27 M. Hainbuchner, M. Villa, G. Kroupa, G. Bruckner, M. Baron, H. Amenitsch, E. Seidl and H. Rauch, *J. Appl. Crystallogr.*, 2000, **33**, 851–854.
28 S. Mazumder, D. Sen, T. Saravanan and P. R. Vijayaraghavan, *J. Neutron Res.*, 2001, **9**, 39–57.
29 V. K. Aswal and P. S. Goyal, *Curr. Sci.*, 2001, **79**, 947.
30 O. Spalla, S. Lyonnard and F. Testard, *J. Appl. Crystallogr.*, 2003, **36**, 338–347.
31 D. Sen, J. S. Melo, J. Bahadur, S. Mazumder, S. Bhattacharya, G. Ghosh, D. Dutta and S. F. D'Souza, *Eur. Phys. J. E*, 2010, **31**, 393–402.
32 A. Thill and O. Spalla, *J. Colloid Interface Sci.*, 2005, **291**, 477–488.
33 D. Sen, A. Khan, J. Bahadur, S. Mazumder and B. K. Sapra, *J. Colloid Interface Sci.*, 2010, **347**, 25–30.
34 J. S. Pedersen, *J. Appl. Crystallogr.*, 1994, **7**, 595–608.
35 S. F. D'souza, J. S. Melo, A. Deshpande and G. B. Nadkarni, *Biotechnol. Lett.*, 1986, **8**, 643–648.
36 L. M. Helander, H. Alakomi, K. Latva-Kala and P. Koski, *Microbiology*, 1997, **143**, 3193–3199.